Catalysis Today 168 (2011) 17–27

Contents lists available at ScienceDirect

Catalysis Today

journal homepage: www.elsevier.com/locate/cattod

Catalytic and molecular separation properties of Zeogrids and Zeotiles

Johan A. Martens[a,*], Joris W. Thybaut[b], Joeri F.M. Denayer[c], Sreeprasanth Pulinthanathu Sree[a], Alexander Aerts[a], Marie-Françoise Reyniers[b], Veronique Van Speybroeck[d], Michel Waroquier[d], Anita Buekenhoudt[e], Ivo Vankelecom[a], Wim Buijs[g], Jeroen Persoons[c], Gino V. Baron[c], Sara Bals[f], Gustaaf Van Tendeloo[f], Guy B. Marin[b], Pierre A. Jacobs[a], Christine E.A. Kirschhock[a]

[a] *Centrum voor Oppervlaktechemie en Katalyse, KU Leuven, Kasteelpark Arenberg 23, B-3001 Heverlee, Belgium*
[b] *Laboratory for Chemical Technology, Ghent University, Krijgslaan 281 – S5, B-9000 Ghent, Belgium*
[c] *Department of Chemical Engineering, Vrije Universiteit Brussel, Pleinlaan 2, B-1050 Brussel, Belgium*
[d] *Center for Molecular Modeling, Ghent University, Technologiepark 903, B-9052 Zwijnaarde, Belgium*
[e] *VITO, Separation and Conversion Technology, Boeretang 200, B-2400 Mol, Belgium*
[f] *EMAT, University of Antwerp, Groenenborgerlaan 171, B-2020 Antwerp, Belgium*
[g] *Catalysis Engineering, Delft Chem Tech, TU Delft, Julianalaan 136, 2628 BL Delft, The Netherlands*

ARTICLE INFO

Article history:
Received 23 November 2010
Received in revised form 21 January 2011
Accepted 24 January 2011
Available online 8 March 2011

Keywords:
Zeogrid
Zeotile-1
Zeotile-2
Zeotile-4
Zeotile-6
Hierarchical materials
Molecular separation
Membranes
Catalysis

ABSTRACT

Zeogrids and Zeotiles are hierarchical materials built from assembled MFI zeolite precursor units. Permanent secondary porosity in these materials is obtained through self assembly of nanoparticles encountered in MFI zeolite synthesis in the presence of supramolecular templates. Hereon, the aggregated species are termed nanoslabs. Zeogrids are layered materials with lateral spacings between nanoslabs creating galleries qualifying as supermicropores. Zeotiles present a diversity of tridimensional nanoslab assemblies with mesopores. Zeotile-1, -4 and -6 are hexagonal mesostructures. Zeotile-1 has triangular and hexagonal channels; Zeotile-4 has hexagonal channels interconnected via slits. Zeotile-2 has a cubic structure with gyroid type mesoporosity. The behavior of Zeogrids and Zeotiles in adsorption, membrane and chromatographic separation and catalysis has been characterized and compared with zeolites and mesoporous materials derived from unstructured silica sources. Shape selectivity was detected via adsorption of n- and *iso*-alkanes. The mesoporosity of Zeotiles can be exploited in chromatographic separation of biomolecules. Zeotiles present attractive separation properties relevant to CO_2 sequestration. Because of its facile synthesis procedure without hydrothermal steps Zeogrid is convenient for membrane synthesis. The performance of Zeogrid membrane in gas separation, nanofiltration and pervaporation is reported. In the Beckmann rearrangement of cyclohexanone oxime Zeogrids and Zeotiles display a catalytic activity characteristic of silicalite-1 zeolites. Introduction of acidity and redox catalytic activity can be achieved via incorporation of Al and Ti atoms in the nanoslabs during synthesis. Zeogrids are active in hydrocracking, catalytic cracking, alkylation and epoxidation reactions. Zeogrids and Zeotiles often behave differently from ordered mesoporous materials as well as from zeolites and present a valuable extension of the family of hierarchical silicate based materials.

1. Introduction

The conventional hydrothermal synthesis of aluminosilicate zeolites typically leads to the formation of micrometer sized zeolite crystals. Traditionally, for operation in adsorptive separation and heterogeneous catalysis these zeolite powders are formed into pellets, tablets and extrudates thus generating macroporosity in between compacted zeolite crystals. While this physical form of zeolite has been successfully applied in many instances, the performance of compacted micron sized zeolite crystals in sometimes can be sub optimal because of inefficient mass and heat transfer. Over the last decade the scientific community has invested heavily in alternative structuring of zeolite matter [1–5]. Limiting the size of the zeolite particles to the nanometer range is an obvious approach to shorten the intracrystalline diffusion path length. Nanosize versions of many types of zeolites have already been synthesized [6]. However, the retention of nanozeolite in a reactor is problematic, and shaping of the nano material in larger bodies is needed for separating the nano zeolite from reaction products. While compaction and fixation of zeolite nanopowder in a random manner similar

* Corresponding author. Tel.: +32 16 321637; fax: +32 16 321998.
E-mail address: Johan.Martens@biw.kuleuven.be (J.A. Martens).

0920-5861/$ – see front matter © 2011 Elsevier B.V. All rights reserved.
doi:10.1016/j.cattod.2011.01.036

Table 1
Overview of synthesis of hierarchical materials based on MFI nanoslabs.

Material	Secondary template	V_{meso} (ml/g)	V_{micro} (ml/g)	Pore shape/size (nm)	Symmetry	Reference
Zeogrid	CTAB in EtOH		Total micropores: 0.69 Ultra micropores: 0.14 Super micropores: 0.55	Slit like pores: 1.4	Layered structure	[14,15,38,42,43]
Zeotile-1	CTAB aqueous	0.76	0.15	Hexagonal pores: 3.5 Triangular pores: 1.4	Hexagonal	[14,16]
Zeotile-2	CTAB powder	0.89	0.09	Gyroid: 2.7	Cubic	[16,46]
Zeotile-4	P123-aqueous	1.27	0.11	Hexagonal channels: 7.5 Slit like pores: 3.3	Hexagonal	[14,16,47]
Zeotile-6	CTAB powder	0.9	0.01	Hexagonal	Hexagonal	

to the micron size powder is an option, the design of hierarchical materials with optimization of porosity at different length scales is an appealing concept. Several approaches are available for generating mesopores in zeolite crystals such as steaming and acid leaching to remove aluminum [7] or desilication with basic solution [8] or the synthesis of the zeolite on hard template which upon removal generates the mesopores [9]. Yet another option is the supramolecular assembly of zeolite nanoparticles. Proto-zeolitic nanocrystals obtained in the nucleation phase of a zeolite synthesis have been assembled into ordered mesoporous materials [10].

Zeolites with MFI topology and especially silicalite-1 have been among the first zeolites for which the synthesis of nanoparticles has been realized [11–13]. The possibility of synthesizing stable suspensions of uniform embryonic zeolite particles via the so called clear solution approach offered a unique opportunity for attempting hierarchical structuring [14]. The design of hierarchical materials from MFI zeolite nanoparticles contained in clear solutions over the past 10 years has been an important research topic in Flanders and resulted in over 20 publications out of collaborative research in the frame of interuniversity attraction poles and strategic basic research programs. The building units of the investigated hierarchical materials are nanoparticle aggregates of uniform size having emerging MFI zeolite type connectivity on a local scale. At the second structural level, these aggregates, referred to as nanoslabs, are linked through their corners, edges or faces following patterns imposed by supramolecular chemistry [15,16]. After evacuation of the molecular and supramolecular templates, microporosity inside and precise mesoporosity between the nanoslabs are obtained. Depending on the nanoslab fixation conditions the mesostructural organization and corresponding mesoporosity can be tuned. With this self-assembly concept the generation of porous bodies is much better controlled compared to the conventional zeolite crystallization methods involving solubility driven nucleation and crystal growth followed by physical shaping. Here we present a review of our publications on the nanoslab approach to hierarchical materials and achievements in the area of materials science, adsorptive separation, membranes and catalysis complemented with new data.

2. Results and discussion

2.1. Building hierarchical materials from nanoslabs

The MFI framework structure is built out of 4-, 5-, 6- and 10-membered rings of T-atoms [17]. The microporosity of MFI framework is characterized by straight channels running in the crystallographic *b* direction and zigzag channels in the *a* direction intersecting with the straight channels. Both channel types are delineated with 10-rings, offering minimum free dimensions of 0.53 nm by 0.56 nm along the straight channels, and 0.51 by 0.55 nm along the zigzag channels (Fig. 1).

Tetrapropylammonium (TPA) is a powerful structure directing agent for the synthesis of MFI type zeolites [18–20]. In the final, fully crystalline, zeolite TPA is located at channel intersections with its four propyl groups residing in different channels. The analysis of the molecular steps leading to formation of the complex MFI topology with 12 different T-atom positions in the orthorhombic unit cell is challenging but understanding is in progress [21,22]. The formation of silicalite-1, the siliceous MFI zeolite, has been intensively investigated under synthesis conditions with varying TPA concentration. Also on theoretical level special graphical tools (ZEOBUILDER) have been developed to build geometries of these nanoparticles and to assist in interpreting the experimentally observed phenomena regarding the nanogrowth process [23–25]. The hydrolysis of tetraethyl orthosilicate (TEOS) in the presence of tetrapropylammonium hydroxide (TPAOH) gives rise to the formation of a stable suspension of nanoparticles [26]. Initial nanoparticle formation is driven by the tendency of the template to form micelles, which leads to aggregation of small silica oligomers in solution encapsulated in a shell of TPA^+ [27–31]. Soon after nanoparticle formation the connectivity of silica within these nanoparticles starts to deviate from oligomers in solution and successively approaches the connectivity found in MFI [31,32]. Over long periods of time at room temperature or at much shorter times during hydrothermal treatment the protozeolitic particles improve their internal ordering to such a degree to become fit for aggregation into crystalline zeolite particles [33–36].

Spreading of the nanoparticles on carbon grid and observation in TEM revealed the formation of slab shape particles with discrete dimensions such as 4 nm × 4 nm [37,38]. Heights of these nanoslabs estimated by AFM correspond to ca. 1.3 nm and its multiples [12]. A theoretical study furthermore revealed the template molecule shows a strong affinity for forming a fragment of the 10R channel of the final zeolite [39]. As within the nanoparticles the

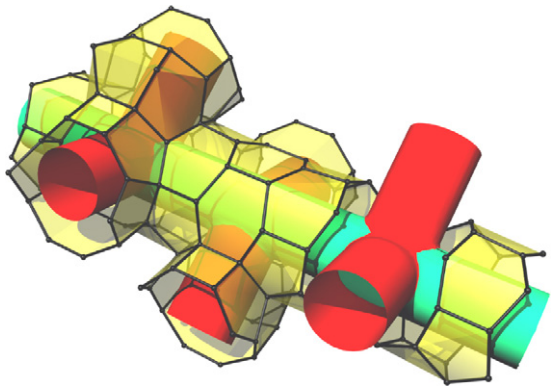

Fig. 1. Pore architecture of MFI zeolite. Straight 10R channels along the *b*-direction are intersected by 10R zigzag channels along *a*. Failure to complete a zigzag channel can result in large openings in the terminating surface.

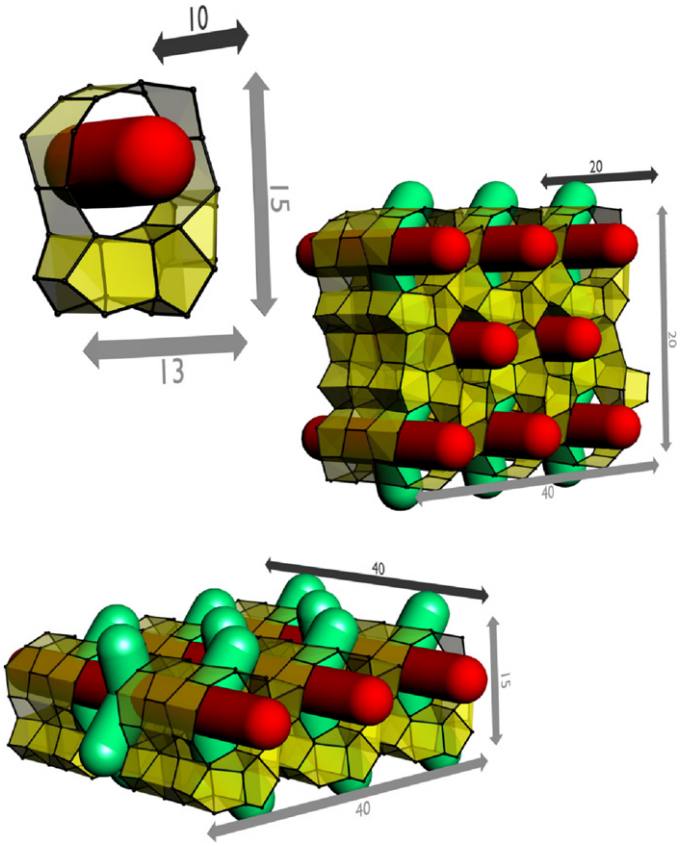

Fig. 2. Representation of idealized precursor and two aggregates (both assembled from 12 precursors). Straight channels are indicated in red, zigzag channels in green. (For interpretation of the references to color in this figure legend, the reader is referred to the web version of this article.)

template molecules reside in intimate contact with silica, eventual formation of such silica-template species appears feasible. Indeed, a solid state NMR study of freeze dried nanoparticle suspension revealed the distances between template and silica species agreed well with such a model of a precursor [40]. Comparison of this precursor structure with the experimentally derived dimensions indicated the observed nanoslabs could result from side by side precursor-aggregation enforced by the sample preparation [33]. Idealized atomic models of the nanoslab containing 3 straight channels and 4 zigzag channels have been presented [13]. Depending on the TPAOH–water–TEOS composition, temperature, pH and presence of secondary mesostructuring template, half nanoslabs, nanoslabs, tablets, staples of tablets and nanozeolite particles have been prepared [13,41,42]. Idealized representations of precursors, and typically encountered aggregates derived therefrom are presented in Fig. 2.

The availability of concentrated suspensions of embryonic zeolite nanoparticles invited the attempt to synthesize hierarchical materials. Concepts adapted from the synthesis of ordered mesoporous materials involving the use of supramolecular templates were adopted. A first type of material coined Zeogrid [15,42,43] was synthesized by precipitation of the precursor suspension upon addition of a saturated solution of cetyltrimethylammonium bromide (CTAB) in ethanol. In Zeogrid the nanoparticles aggregate into layers which then are stacked concentrically, intercalated by surfactant molecules. The final porous structure is obtained after burning out the TPA and CTAB through calcination (Fig. 3, bottom). In a Zeogrid the layer repeat distance is ca. 3.0 nm. Zeogrid has a dual microporosity. Ultramicropores typical of MFI zeolite framework are located inside the nanoslabs, while the spacing between slabs

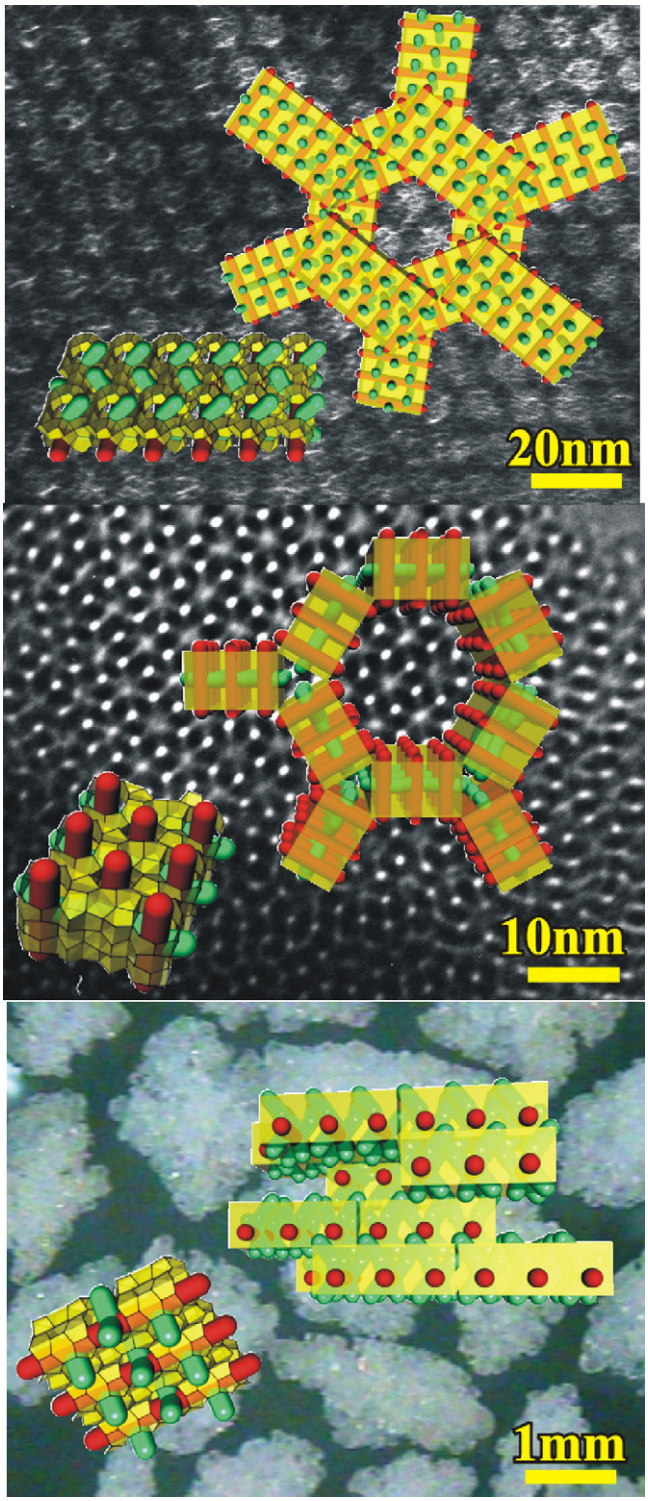

Fig. 3. Tiling patterns of nanoslabs in Zeogrid (bottom) and Zeotile materials top: Zeotile-4, middle: Zeotile-1. Images are superimposed on TEM and optical micrographs.

qualifies as supermicroporosity. The height of the galleries estimated by modeling of N_2 adsorption isotherms was ca. 1.4 nm, in agreement with the thickness of an individual layer height [44,45]. Representative ultramicropore and supermicropore volumes are reported in Table 1.

Zeotiles [16,46,47] are another class of materials in which the aggregation of nanoparticles and subsequent linking of nanoslabs

is fully ordered (Fig. 3, top and middle). When water is used as solvent for CTAB, Zeotile-1 is obtained by precipitation from a precursor suspension. In the structure of Zeotile-1 the dimensions of the resulting nanoslabs agree with units composed of face-sharing double precursors measuring 2.6 nm × 2.0 nm × 4.0 nm. The assembly of these building blocks in a hexagonal pattern imposed by the CTAB gives rise to hexagonal and triangular channels. Triangular channels are unique in mesoporous materials science. Their formation in the presence of CTAB is a natural consequence of the tiling of the formed monodisperse aggregates of 12 nanoslabs (Fig. 2, right) under these conditions. The hexagonal channels have a free diameter of 3.5 nm and the triangular channels of 1.4 nm.

Yet two further ordered tiles, Zeotile-2 and -6 are obtained by adding CTAB powder to the nanoslab suspension, while essentially retaining the pH of the native nanoparticle suspension. As no rapid aggregation of the precursor particles is initiated by lowering pH, nanoparticle arrangement now was observed to follow topologies typical for CTAB as the mesostructuring agent, also encountered when using unstructured silica sources. Zeotile 2 obtained at high temperatures has a body centered cubic symmetry and contained mesopores having an average diameter of ca. 2.7 nm. Zeotile-6, obtained at lower temperatures, shows the typical hexagonal ordering observed for a number of mesoporous materials derived from CTAB. The quality of the ordering can be appreciated from the TEM images and XRD patterns presented in Figs. 4 and 5 and from the narrow mesopore size distribution in Fig. 6. Even though these two materials at first sight resemble traditional mesoporous silica they still retain characteristics of local MFI connectivity as separation studies demonstrated (vide infra).

The synthesis of Zeotile-4 was inspired by SBA-15 preparation. A clear suspension of precursor nanoparticles was acidified to pH 0 using concentrated HCl and then combined with acidified triblock copolymer Pluronic P123 solution followed by hydrothermal ageing at 90 °C. The templates were removed by calcination. The structure at the meso scale has been determined using electron tomography. In Zeotile-4 a 3D mesoporosity is achieved via stapling and annealing of precursor aggregates measuring ca. 8 nm × 4 nm × 1.7 nm. The specific nanoslab organization in Zeotile-4 creates about 7.5 nm wide hexagonal parallel channels connected in four directions via 3.3 nm wide slits [16,47].

The introduction of aluminum atoms in the tetrahedral network of MFI zeolite precursor composing the nanoslab has been demonstrated [40] and the position of the heteroatom has been

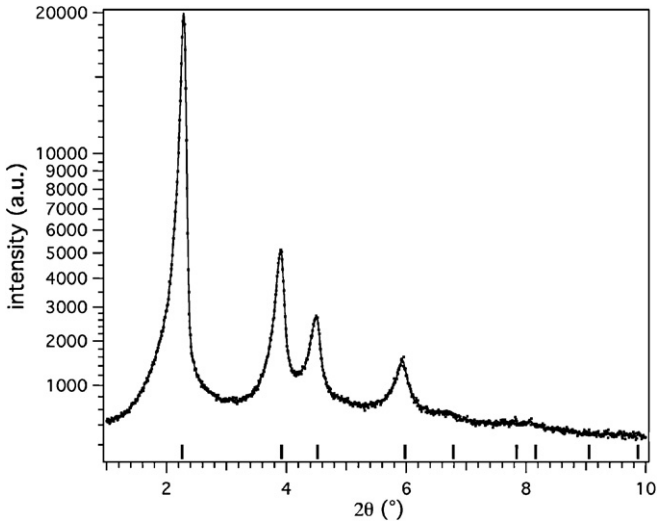

Fig. 5. Reflection powder XRD pattern of calcined Zeotile-6. Pattern can be indexed in the P6mm hexagonal space group, with $a = 4.5$ nm and $c = \infty$.

speculated about [48]. Nanoslabs and materials derived thereof with Si/Al ratio of 50 are conveniently prepared. Reichinger et al. composed a hexagonal Zeotile out of titanosilicate nanoslabs [49]. The IR signature of MFI framework [32] was detected. The presence of microporosity was deduced from the presence of TPA in the walls of the mesopores and the presence of specific surface areas that were significantly larger than expected if mesopore walls were dense.

2.2. Adsorption properties of Zeogrids and Zeotiles

The molecular sieving properties of Zeogrids have been demonstrated using pulse gas-chromatographic separation of alkane mixtures. In binary mixtures of alkanes of different branches such as n-octane and 2,2,4-trimethylpentane, and of n-heptane and 2,3-dimethylpentane, the linear molecule is preferentially adsorbed. Preferential adsorption of the slender molecule is a manifestation of molecular shape selectivity in ultramicropores [15], and normally absent in traditional mesoporous silica. Micron size MFI zeolites separate branched from normal alkanes irrespective of carbon number. On Zeogrids, when the branched alkane is heavier

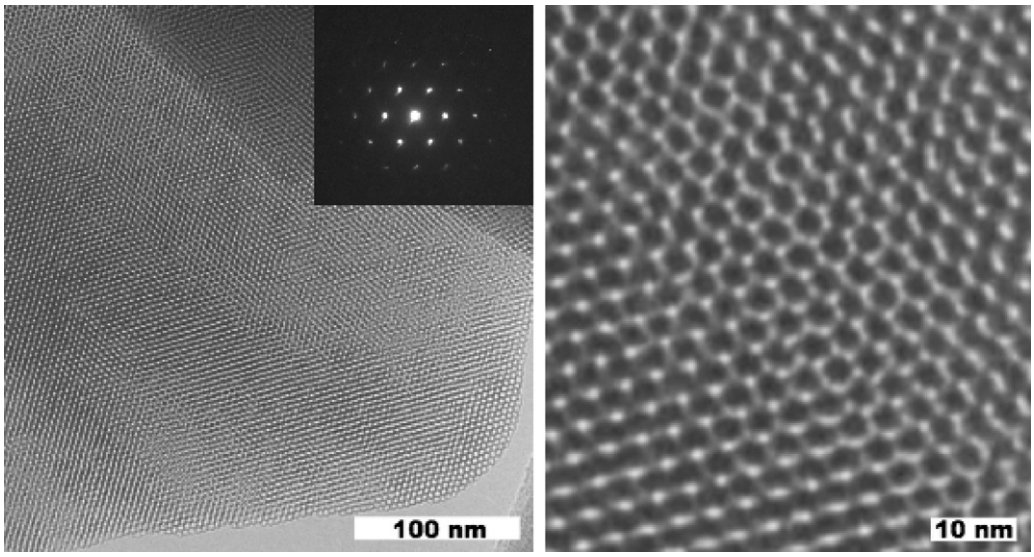

Fig. 4. TEM images of Zeotile-6. (Left) Overview and (right) detail. Inset in left image: ED pattern.

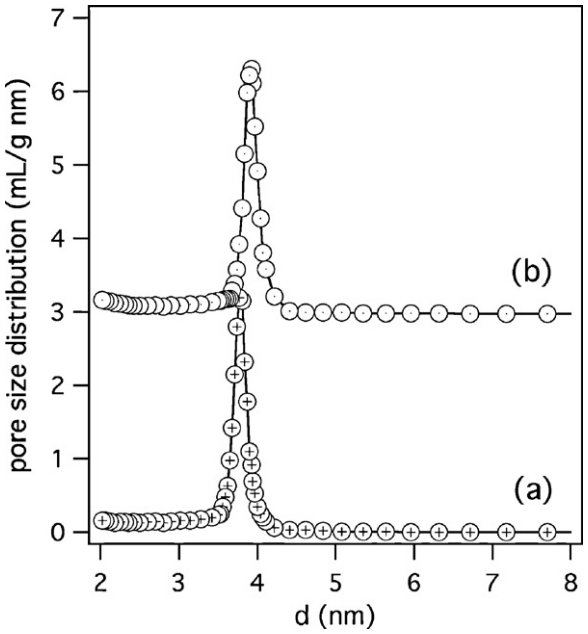

Fig. 6. BJHKJS pore size distributions of (a) Zeotile-6 from which CTAB was removed by template extraction and (b) calcined Zeotile-6.

than the linear one, the branched alkane is selectively adsorbed. This behavior different from the MFI zeolite is due to contributions of the supermicropores in the adsorption of mixtures. The supermicropores discriminate among molecules based on molecular weight, while in ultramicropores the discrimination is based on branchiness. The presence of two adsorption environments in ultramicropores and supermicropores, the contribution of which can be tuned by the size of the zeolite building blocks composing the Zeogrid, enables fine-tuning of adsorption behavior. An important observation was that mass transfer resistances in Zeogrid columns were much lower than in conventional ZSM-5 columns [15]. The presence of supermicroporosity in Zeogrid is at the origin of the reduced mass transfer resistance.

Zeotile-2 enabled the pulse chromatographic separation of n-octane and *iso*-octane [50]. n-Octane was longer retained in the Zeotile-2 column compared to *iso*-octane. The selective adsorption of the linear alkanes was ascribed to adsorption in ultramicropores. In a more extensive investigation of C_5–C_9 n- and *iso*-alkane adsorption, it was demonstrated that whereas MCM-48 did not show any shape selectivity, Zeotile-2 exhibited shape selective discrimination among n- and *iso*-alkanes. The preferential adsorption of n-alkanes in Zeotile-2 is an entropic effect. *Iso*-alkanes in adsorbed state were found to have limited freedom explained by adsorption in the confined environment of a micropore. Thus Zeotile-2 was interpreted as a hierarchical variant of MCM-48, presenting microporosity in the walls of the gyroid type mesostructure [46].

In another application, spherical bi-porous Zeotile-4 particles were synthesized and used as stationary phase in high performance liquid chromatography for the separation of biomolecules. Although it has been shown that zeolites are good candidates for the purification of nucleic acids and proteins [51], they suffer from slow diffusion inside their small pores ($\leq$10 Å), certainly in liquid phase applications where mass transfer often plays a crucial role. Mesoporous materials such as MCM-41 have already been used in chromatography applications, but use of hierarchically ordered materials with micro and mesoporosity has not been reported so far [52–58].

We used the nanometer sized zeolite slabs as silicon source to generate spherical particles with well-defined mesoporosity,

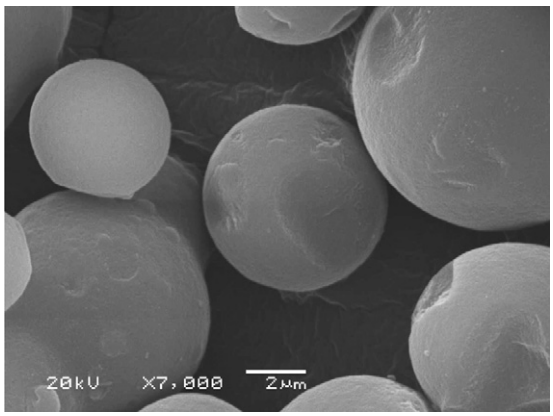

Fig. 7. SEM images of spherical Zeotile-4 particles for HPLC applications.

suited for HPLC applications. Retention characteristics of the prepared materials were studied by using a group of brain peptides in hydrophilic interaction chromatography (HILIC). HILIC provides an alternative approach to effectively separate small polar compounds on polar stationary phases. Similar to normal phase liquid chromatography (NPLC), polar compounds are more strongly retained in HILIC, but the non-aqueous mobile phase in NPLC is replaced with an aqueous–organic mixture with water being the stronger solvent [59].

Spherical Zeotile-4 particles were prepared under acidic conditions, starting from large nanoslabs with dimensions of 1.3 nm × 4.0 nm × 8.0 nm, obtained through acidification of nanoslab suspension. Triblock copolymer and CTAB served as tiling agent for Zeotile-4 materials. The TPA, copolymer and CTAB were evacuated from the solid material through calcination. SEM images for the Zeotile-4 product show spherical particles (Fig. 7), with a diameter between 3 and 10 μm. N_2 porosimetry showed a pore size profile with narrow pore size distribution, centered on 7.15 nm. The BET surface area and total pore volume of the spherical Zeotile-4 were determined to be 970 $m^2\,g^{-1}$ and 1.35 $cm^3\,g^{-1}$, respectively. The large capacity and surface area could be beneficial for chromatographic separation.

In order to study the performance of spherical Zeotile-4 as stationary phase in HPLC, a slurry packed column (300 mm × 4.6 mm) was tested in HILIC experiments. Fig. 8 illustrates the HILIC chromatographic profile for a group of tyrosine-containing peptides

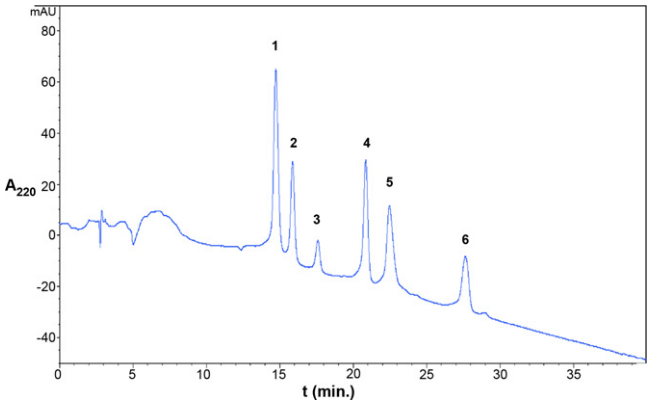

Fig. 8. Chromatogram of a mixture of six brain peptides separated on a Zeotile-4 column (300 mm × 4.6 mm); mobile phase: acetonitrile (0.2 vol.% trifluoroacetic acid, TFA) and water (0.2 vol.% TFA). Peptide separation gradient for 2–60 min with acetonitrile (0.2 vol.% TFA) changed from 99% to 60%. The model peptides have the following structure: (1) Tyr-Ala-Gly-Phe-Met, (2) Tyr-Gly-Gly-Phe-Met, (3) Tyr-Ala-Gly-Phe-Met-o, (4) Tyr-Met-Gly-Phe-Pro-NH_2, (5) Tyr-Ala-Arg-CH_3COOH and (6) Tyr-Ala-Gly-Phe-Met (O)-ol.

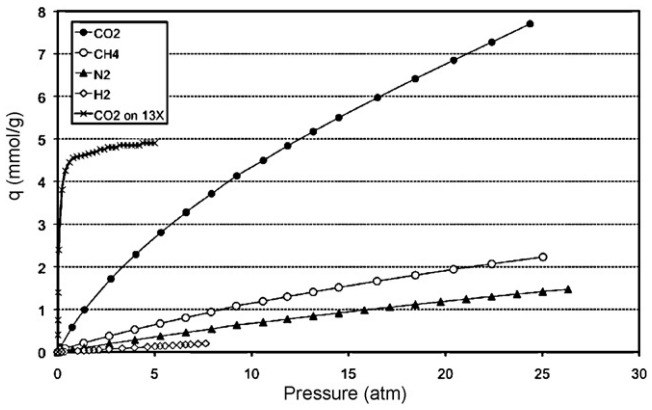

Fig. 9. Adsorption isotherms of CO_2, CH_4, N_2 and H_2 on Zeotile-2 at 25 °C. The adsorption isotherm of CO_2 on 13X zeolite is added as a reference.

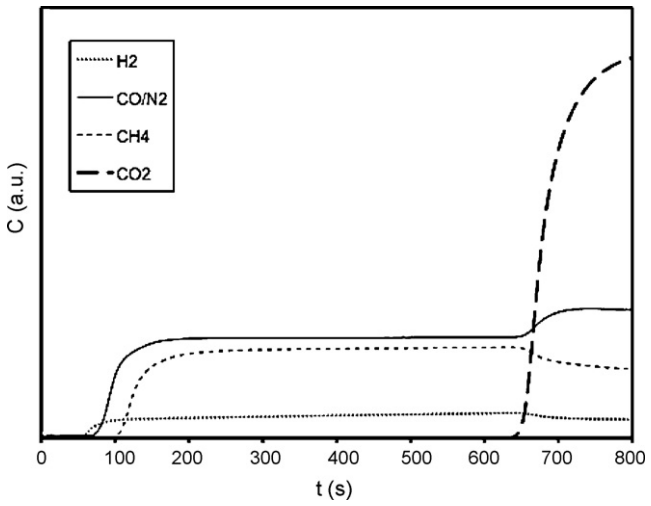

Fig. 10. Breakthrough profile of a gas mixture containing CO_2, CH_4, N_2 and H_2 separated on a column packed with Zeotile-2 pellets, at 25 °C and 1 atm.

(1–6) in the effluent fraction. Four of the six brain peptides contain met-enkephalin peptides. A 60-min linear gradient of acetonitrile (99–60%) and water (1–40%) with 0.2 vol.% trifluroacetic acid (TFA, as the acid modifier) was used for the separation of brain peptides.

Six well-resolved peaks in the chromatographic trace are observed (Fig. 8), demonstrating that the brain peptide mixture has been separated very well on the Zeotile-4 HPLC column. Each component of the mixture shows an almost symmetrical peak (Fig. 8). It seems that the hydrophilic/hydrophobic character of the analytes is the most important factor in their separation. The met-enkephalin peptides (1, 2 and 6) with a different functional group elute at very different elution times, although they have the same amino acid sequence. The presence of different functional groups attached to the peptides of same amino acid sequence leads to change the hydrophilicity of the peptides.

Thus, spherical Zeotile-4 is a promising stationary phase for peptide separation in liquid chromatography, and is expected to be of use in the separation of various biomolecules. The material is very stable and could be used repeatedly without losing any activity.

Given the large pore volumes of the hierarchical materials built from nanoslabs, we further studied adsorption of CO_2 and other gases on Zeotile-2. There is great interest to develop technologies to sequester CO_2 and limit its effect on climate. The separation of CO_2 from natural gas, landfill gas or biogas is important to obtain a CH_4-enriched stream since CO_2 not only reduces the energy content of the gas but can corrode pipelines as well. Development of successful separation technologies for removal of CO_2 from a variety of gas streams is still a challenging research topic. Adsorption processes have been suggested as an alternative to conventional processes such as amine absorption, amine scrubbing, and distillation [60].

To illustrate the preference in adsorption, Fig. 8 shows the adsorption isotherms of CO_2, CH_4, N_2 and H_2 at 25 °C on Zeotile-2. Carbon dioxide is definitely adsorbed the strongest with a capacity 3–4 times larger of that of methane. Methane from its part is still adsorbed stronger on Zeotile-2 compared to nitrogen and finally hydrogen. Although Zeotile-2 adsorbs significantly less CO_2 than 13X zeolite at low pressure (see Fig. 9), its capacity at higher pressure is significantly larger. The separation power of Zeotile-2 was tested by performing breakthrough experiments using a column packed with Zeotile-2 pellets. From Fig. 10, it can be clearly observed that Zeotile-2 allows separation of CO_2 from its mixture with CH_4, H_2, CO and N_2.

2.3. Zeogrid membranes

Zeolite membranes are of interest to gas separation, pervaporation and nanofiltration. Currently there is also a renewed interest in catalytic membrane reactors for coupling reaction and product separation such as in Fischer–Tropsch synthesis. Traditional synthesis of zeolite membranes via hydrothermal crystallization often leads to inter-crystalline defects in the membranes, a problem that is encountered especially at large scale production [61]. Inter-crystalline defects, pinholes and cracks inevitably deteriorate the molecular sieving properties of the zeolite membrane. The difficulty to produce defect-free membranes is a major reason why only a small number of zeolite membranes became commercially available.

The synthesis of a Zeogrid does not involve any hydrothermal step. The interposed stapling of nanoslabs to create a top layer of an asymmetric membrane is an attractive approach for synthesizing a zeolite-membrane (Fig. 11). The challenge consists in achieving perfect nanoslab stacking with sufficient adhesion to the porous support after removal of the surfactant molecules.

Provided the perfect stacking of nanoslabs sketched in Fig. 11 can be achieved, any molecule approaching the membrane will need to diffuse through a zeolite micropore of a nanoslab, similar as in standard zeolite membranes. Consequently, defect-free new membranes are estimated to have a similar selectivity as the standard zeolite membranes. However, the presence of the supermicropores in the top layer can lead to membranes with a much higher permeability. Moreover, the Zeogrid approach can enable the preparation of ultra-thin membrane top layers. Therefore, the Zeogrid approach of membrane preparation presents the potential to combine high separation power with extra high permeation.

Preliminary experiments for evaluating the feasibility to form Zeogrid top layers were performed on silicon wafers. Hereto a solution of silicalite nanoslabs was mixed with CTAB, as done in the synthesis of Zeogrid powder. A droplet of this mixture was spread

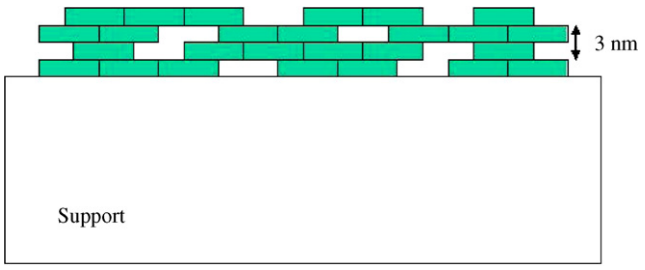

Fig. 11. Zeogrid top layer on a porous support forming a composite zeolite membrane.

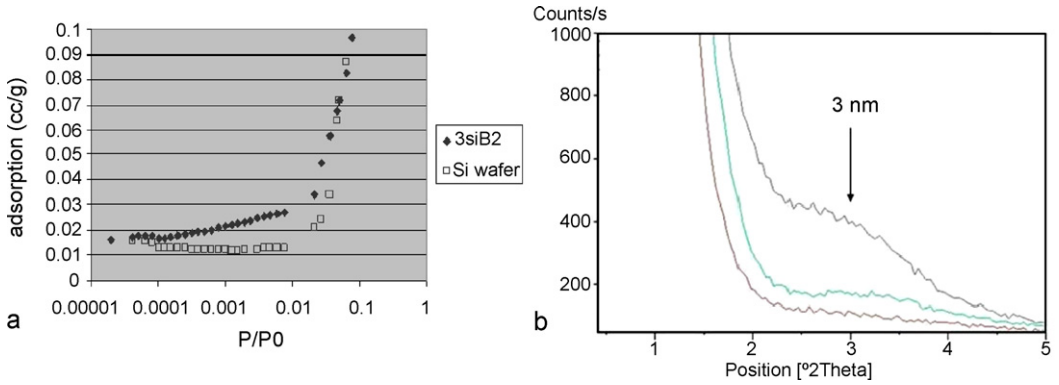

Fig. 12. (a) Adsorption isotherms of a two-layer silicalite nanoslab membrane on silicon wafer ($3SiB_2$) and of a bare silicon wafer, and (b) low-angle XRD of a two-layer silicalite nanoslab membrane on silicon wafer (upper curve), a one-layer silicalite nanoslab membrane on silicon wafer (middle curve), and a bare silicon wafer (lower curve).

out on a small piece of polished silicon wafer, dried and calcined at the appropriate temperature to remove the surfactant. Sometimes this procedure was repeated in order to increase the thickness of the layer. The N_2-adsorption isotherm of Zeogrid deposited in two layers on silicon wafer is shown in Fig. 12a. Nitrogen uptake in ultramicropores occurs at very low P/Po values below 10^{-4}. The upswing of the isotherm starting around P/Po of 0.1 is due to the filling of supermicropores. A similar isotherm shape was observed on Zeogrid powder. Low-angle XRD (Fig. 12b) of single and double Zeogrid layers revealed a reflection maximum near $2\theta = 3^\circ$ corresponding to a repeat distance of ~3 nm. This ~3 nm repeat is characteristic of Zeogrid and is linked with the thickness of two nanoslabs.

Zeogrid coatings were deposited on porous alumina supports (flat and tubular, support pore size 50–100 nm). In order to prevent intrusion of the nanoslabs into the pore system of the supports, all supports were first coated with one or two intermediate colloidal titania sol–gel layers [62]. These intermediate layers decrease the pore size to about 2 or 3 nm corresponding to a molecular weight cut-off value of ~4 kDa. Zeogrid coatings were applied via dip-coating of flat or tubular supports. Coatings were carefully dried and calcined at the appropriate temperature to remove the surfactant. Typical SEM pictures of these membranes (Fig. 13) confirmed the formation of a continuous top layer.

The Zeogrid membranes were evaluated in nanofiltration of mixtures of small PEG molecules with molecular weights of 200, 600 and 1500 Da, respectively. Provided a defect-free Zeogrid layer was present, very low water permeability was expected due to the

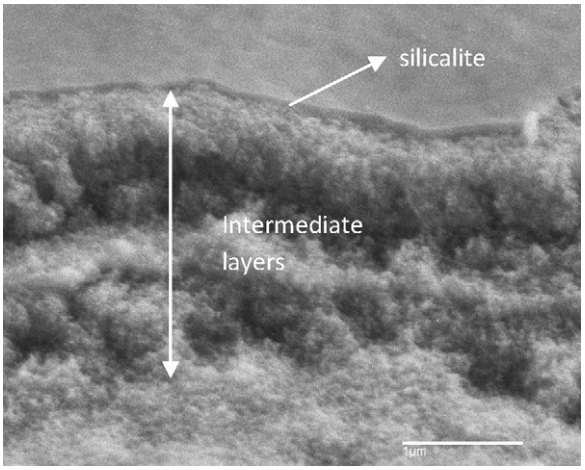

Fig. 13. SEM picture of the cross section of a typical silicalite nanoslab membrane on a porous support. The bar measures 1 μm.

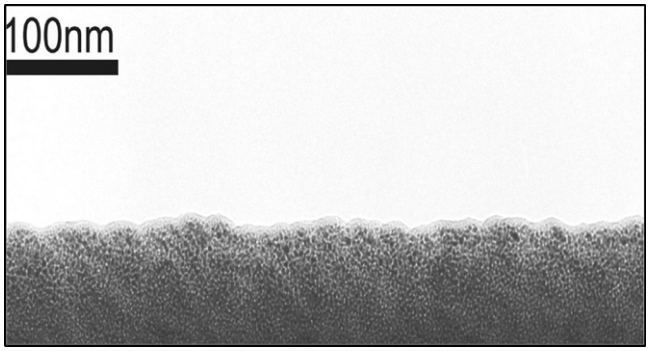

Fig. 14. TEM picture of the cross section of a typical Zeogrid membrane on silicon wafer.

hydrophobicity of the silicalite type micropores, and a membrane molecular weight cut-off <200 Da due to the size of the silicalite pores of ~0.5 nm. Typical water permeabilities on tubular membranes were 5 l/hm^2 bar with molecular weight cut-offs of about 1000 Da. This result revealed that the deposited Zeogrid was not perfect. Investigation with TEM of a piece of Zeogrid layer sample on silicon wafer prepared using FIB (Fig. 14) confirmed the imperfect nanoslab stacking.

The performance of the membranes in pervaporation of different organic solvent/water mixtures was evaluated (Table 2). The performance of standard silicalite membranes, measured in the same mixtures is also given (between brackets). From the table it is clear that our new type of silicalite membrane, despite their non-ideal quality, shows a clear organophilic behavior, like the standard silicalite membrane. This means that the permeating stream definitely experiences the zeolitic micropores inside the nanoslabs, and that the non-zeolite pores are probably small (order of 1 to a few nm). Indeed, the stacking pores in between the nanoslabs are hydrophilic in nature (see Section 2.1) and would rather lead to non-selective or de-watering behavior. This conclusion is also subscribed by comparing the results of a homemade nanoporous hydrophilic titania nanofiltration membrane with a molecular

Table 2
Pervaporation performance of a Zeogrid membrane at room temperature in different alcohol/water mixtures. The results between brackets show the performance of a standard silicalite membrane under similar conditions.

Mixture	Selectivity α	Organic concentration Feed → permeate	Flux (kg/m^2 h)
Ethanol/water	2.9 (25)	6% → 15%	20 (1)
Isopropanol/water	2.7 (25)	2.5% → 6.5%	20 (0.1)
Acetone/water	4.8 (100)	2.5% → 11%	15

Table 3
Mixed gas separation performance of a silicalite nanoslab membrane at room temperature in different gas mixtures. Trans membrane pressure was low (1–2 bar). The results between brackets show the Knudsen selectivities.

Gas mixture	Selectivity α	Permeability (m^3/hm^2 bar)
N_2/CO_2 88/12	0.6 (1.25)	3
H_2/CO_2 40/60	1.7 (4.7)	9

weight cut-off of 200 Da (pores <1 nm). This membrane showed no selectivity in any of the mixtures. Compared to the standard silicalite membranes, the new type of membranes showed lower separation values (due to the non-zeolite pores) and much higher fluxes.The new type of membranes was also tested in gas separation measurements. Single gas measurements of N_2, H_2 and CO_2 showed high permeabilities, proportional to the transmembrane pressure, and increasing with temperature (measured between room temperature and 200 °C). The permselectivities were close to the Knudsen selectivities, as could be expected due to the existence of small non-zeolite pores. However, as can be seen in Table 3, mixed gas separation tests revealed selectivities clearly different from Knudsen (Knudsen values shown between brackets in the table). The values show that in a mixture of N_2 and CO_2, this new type of membrane, in contrast to standard silicalite membranes, selectively removes the CO_2 from the gas stream. This is a consequence of the strong CO_2 adsorption of the Zeogrid-type of material, as was previously shown in Section 2.2, and is due to the high amount of hydrophilic stacking pores in between the nanoslabs. The effect of CO_2 adsorption was also seen in the H_2/CO_2 gas mixture. This feature could make these membranes, when optimized, interesting in post-combustion CCS (carbon capture and storage) schemes.

2.4. Catalytic properties of Zeogrids and Zeotiles

2.4.1. Hydrocracking

The isomerization and hydrocracking, or in short the hydroconversion of model long chain n-alkanes such as decane is an attractive catalytic test reaction for probing zeolite pore architectures. At the same time the evaluation of a new material for this reaction is relevant to large scale industrial catalytic processes such as dewaxing through skeletal isomerization and hydrocracking processes.

The decane hydroconversion reaction has been performed on Zeogrid materials [44,45] with aluminosilicate composition and spiked with a trace of platinum metal to achieve bifunctionality. The bifunctional Zeogrids were less active than reference ZSM-5 catalysts. Nevertheless, distinct selectivity patterns were obtained. ZSM-5 zeolite is a medium pore zeolite with pronounced shape selectivity. In hydroisomerization of long n-alkanes Pt/ZSM-5 shows an enhanced selectivity for methyl branching at the C_2 position, and suppresses the formation of skeletal isomers with ethyl branching and with more than one branching [63]. The hydrocracking product distribution of decane on Pt/ZSM-5 is peculiar as it presents a minimum at C_5 [64]. The suppressed cracking of C_{10} molecules in their middle is a manifestation of cage and window effects [65]. Zeogrid do not show the shape selectivity typical of ZSM-5 zeolites. The methyl branching selectivity is typical of large pore zeolites, with kinetic suppression of 2-methylnonane formation. Ethyloctane isomers are formed in significant amounts. Furthermore, there was no suppression of hydrocracking in the middle of the C_{10} molecule. In a comparative study an MFI crystal was composed of aluminosilicate nanoslabs. A selectivity pattern in decane hydroconversion similar to that obtained with the Zeogrids was observed. Materials composed of MFI nanoslabs offer catalytic environments devoid of the shape selectivity of conventional MFI type zeolites.

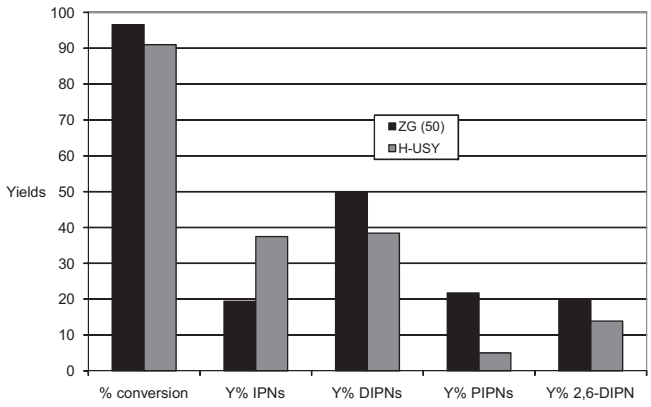

Fig. 15. Product distribution over ZG (50) and H-USY in the isopropylation of naphthalene. Batch type reaction in 50 ml stainless steel Parr autoclave; 2.5 mmol naphthalene, 5.0 mmol 2-propanol, 25 ml of cyclohexane solvent and 500 mg of catalyst heated 24 h at 200 °C.

The common property of the freshly assembled nanozeolites and Zeogrids is the exposure of faces exposing openings giving access to zigzag channels not confined. Molecular models revealed these pockets are not confined by 10-rings and offer significantly more free space to reacting molecules compared to openings of the straight pore system (Fig. 1). In this respect the nanoslabs resemble MCM-22 zeolite, in which surface pockets are loci of catalytic activity [44,45] in the bifunctional conversion of decane, isomerization and hydrocracking are consecutive reactions. The yield of the skeletal isomerization of the feed n-alkane being an intermediate reaction product is always limited. The isomerization yield from Zeogrids and the nanozeolite assembled from nanoslabs was up to 70%, which is among the highest values reached with large pore zeolites [66]. The peculiar morphology of nanozeolite composed of stapled nanoslabs transformed into conventional crystal shape upon ripening in the synthesis medium. The nanozeolite exhibited shape selectivity typical of ZSM-5, confirming the framework termination mode to be critical [44].

2.4.2. Naphthalene diisopropylation

Selective diisopropylation of naphthalene to 2,6-diisopropylnaphthalene (2,6-DIPN) is an important step in the synthesis of 2,6-naphthalene dicarboxylic acid. Zeolites, and especially ultrastable Y (USY) and mordenite have been reported to be the best catalysts for this reaction [67]. Zeogrid turned out to be an even superior catalyst for this reaction. A comparison with one of the best known catalysts, viz. USY, is presented in Fig. 15. The diisopropylnaphthalene (DIPN) isomer distribution obtained on the two catalysts is presented in Table 4. Both catalysts showed a similar conversion, but Zeogrid yielded significantly more

Table 4
Experimental DIPN isomer distribution over USY and Zeogrid in the isopropylation of naphthalene at 200 °C after 24 h.

Compound	USY	Zeogrid
1,3-DIPN	3.8	8.9
1,7-DIPN	4.9	6.4
2,3-DIPN	0.4	0.8
2,6-DIPN	40.3	38.4
2,7-DIPN	42.9	38.1
1,6-DIPN	7.6	7.1
1,5-DIPN	0.1	0.4
1,4-DIPN	0.1	n.d.

n.d., not detected.

Table 5
Selectivities of saturated and unsaturated products, linear and branched products and of cracked products per carbon number obtained on USY zeolite (FAU; Si/Al_{bulk} = 2.6), ZSM-5 zeolite (MFI; Si/Al_{bulk} = 40) and Zeogrid (Si/Al_{bulk} = 50) at 748 K, 7 kPa *iso*-octane partial pressure and 2 mol% *iso*-octane conversion.

	FAU	MFI	Zeogrid
Saturated	88	83.5	82
Unsaturated	147	180	162
Linear	94	210	102
Branched	141	53.5	106
C_1	17	39	14
C_2	1	40	7
C_3	31	100	45
C_4	177	68	134
C_5	9	16.5	7

diisopropylated (DIPN) and polyisopropylated (PIPN) products, and the desired 2,6-DIPN in particular. Apparently, the Zeogrid with its large volume of supermicropores (Table 1) and the wide surface pockets revealed in decane hydroconversion presented in previous section allows over-alkylation more easily than USY zeolite presenting ultramicropores and mesopores.

2.4.3. Catalytic cracking

Crude oil refiners are faced with the need of upgrading ever heavier feedstock. The diffusion of the heavy molecules in the catalyst pores is more and more a limiting factor in achieving the desired conversion and selectivity levels. The paradigm in FCC catalyst design is that mesoporosity is needed to achieve a precracking of large molecules, while the zeolites develop the highest cracking activity and govern the selectivity. The ultra-stable Y zeolite (USY) presenting unordered intracrystalline mesoporosity is the reference catalyst in fluid catalytic cracking (FCC). It is assumed to be lacking molecular shape selectivity meaning that the access to and reaction at the active sites is, in principle, not restricted by the shape and size of the molecules. In catalytic cracking, such behavior leads to a rather wide product distribution, i.e., ranging from products as light as LPG (C_3–C_4), over gasoline to middle distillates. The addition of medium pore zeolites, and especially medium pore zeolites such as ZSM-5 to the FCC catalyst formulation is practiced for tuning the product distribution towards to market demand. The addition of a shape selective zeolite has a positive effect on the gasoline octane number and propylene yield.

Potential shape-selective effects in catalytic cracking catalysts have been investigated by reaction of 2,2,4-trimethylpentane, also denoted as *iso*-octane, and methylcyclohexane on Zeogrid and reference ultrastable Y zeolite (FAU) and ZSM-5 (MFI) zeolite [68,69]. With bulky *iso*-octane significantly lower site time yields were obtained on the MFI zeolites compared to the FAU zeolites, whereas with methylcyclohexane site time yields on both types of zeolites were in the same range. Slow diffusion of *iso*-octane in the MFI pore structure has been identified to be at the origin of these observations, whereas the diffusion of methylcyclohexane through the MFI pores is not limiting its conversion rate. Site time yields obtained on Zeogrid were significantly lower. In this demanding reaction, the absence of long range framework ordering in Zeogrid was assumed to be responsible for weaker acid strength and lower catalytic activity.

Within a zeolite framework topology, the acid properties were found not to impact the selectivities obtained in the cracking of *iso*-octane nor of methylcyclohexane [68,69]. Differences in *iso*-octane selectivity between FAU and MFI frameworks have been identified that allow interpreting the observed cracking behavior on the Zeogrid material in terms of importance of elementary reaction families and location of the active sites (Table 5). The large pore network of a FAU zeolite does not impose any constraints on bimolecular reactions such as hydride transfer and, hence, the product distribution obtained on a FAU zeolite exhibits the typical features of the corresponding reaction network, i.e., relatively high yields of branched and saturated products [70,71]. On the MFI zeolite, on the contrary, higher selectivities towards linear and unsaturated products were observed. Moreover, the selectivities towards products in the range C_1–C_3 was much higher on the MFI than on the FAU zeolite. Due to the confined structure of the narrower ultramicropores of the MFI structure, bimolecular hydride transfer reactions are sterically hindered by transition state shape selectivity and, correspondingly, protolytic scission is taking over as the most dominant reaction inside the MFI pores. The Zeogrid exhibits a product distribution resembling that of a FAU zeolite, e.g., a high selectivity to C_4 products as well as a relatively high selectivity towards branched products. As a result, it can be inferred that the active sites of Zeogrid are situated in the supermicropores and, hence, that the *iso*-octane conversion should not be limited by diffusion limitations. The fact that the *iso*-octane cracking activity on Zeogrid is, nevertheless, similar to that on the benchmark MFI zeolite indicates the weak acidity of the active sites, as observed already in the methylcyclohexane cracking results, see above.

Table 6
Catalytic properties of titanosilicate Zeogrid and reference materials in the liquid phase epoxidation of (cyclo) hexene with *tert*-butylhydroperoxide in decane.

Catalyst			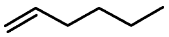	
	X (%)	$S_{epoxide}$ (%)	X (%)	$S_{epoxide}$ (%)
Zeogrid	17	95	11	95
TS-1	0.3	95	1	–
TiMCM-41	6	95	7	–

Reaction conditions: 0.9 M (cyclo)hexene in decane, 0.45 M *tert*-butylhydroperoxide, 90 °C, 24 h, 30 mg catalyst.

2.4.4. Partial oxidation reactions

Ti doped Zeogrid and Zeotile-2, -4 and -6 showed high activity and high epoxide selectivity (Table 6) in the reaction with 1-hexene and cyclohexene, using *tert*-butylhydroperoxide (TBHP) in apolar solvent (decane) [49]. Using H_2O_2 in the polar solvent methanol, activity and epoxide selectivity in (cyclo) hexene epoxidation were lower, and Ti leaching into the reaction medium was observed. The catalytic activity in hydrophilic medium was only a little better than that of Ti doped MCM-41, and much lower than with TS-1 [72,73].

Zeotiles and Zeogrids have been evaluated as catalysts for the vapor phase Beckmann rearrangement of cyclohexanone oxime. The nanoslab based materials typically afforded >99% conversion with a selectivity to ε-caprolactam of 82–89%, which is equivalent to the performance of reference silicalite-1 catalyst [74]. The shape selectivity of the MFI zeolite pore architecture has been thought to be essential for achieving high selectivity in this particular reaction. After 36 h on-stream the conversion was still >90%. Zeotile and Zeogrid catalysts could be regenerated by oxidation in a stream of O_2 at 350 °C. In this reaction, the MFI zeolite properties of the Zeogrids and Zeotiles were exploited.

3. Conclusions

In adsorption and diffusion Zeogrids and Zeotiles display a combined effect of ultramicroporosity in nanoslabs and supermicroporosity and mesoporosity in interstitial spaces. The presence of micropores gives rise to molecular shape selectivity in the separation of mixtures of linear and branched alkanes. The hydrophobicity of the micropores is evident from pervaporation experiments with alcohol/water mixtures. The ultramicropores and mesopores lower the mass transfer resistance compared to zeolite materials in chro-

matographic packings and membranes. The precise mesoporosity and the availability of micron size spherical particles enabled chromatographic separation of peptide mixtures. Removal of CO_2 from gas mixtures using Zeotile-2 or Zeogrid membrane is an attractive feature.

Aluminosilicate and titanosilicate versions of Zeogrids and Zeotiles are active in heterogeneous catalysis. In the hydroisomerization of decane and selective diisopropylation of naphthalene to 2,6-diisopropylnaphthalene Zeogrids are more selective than ultrastable Y zeolite reference. In these acid catalyzed conversions of relatively large molecules the wide surface pockets of nanoslabs composing the Zeogrid are thought being the responsible for the superior catalytic behavior. A weaker acidity in nanoslab based materials compared to fully grown zeolite crystals revealed in catalytic cracking can be tentatively explained by a relaxation of bonds in zeolitic particles measuring hardly 1.4 nm in one dimension. In epoxidation reactions of 1-hexene and cyclohexene with tertiary butyl peroxide in hydrophobic media, titanosilicate Zeogrids are active catalysts. In the Beckmann rearrangement of cyclohexanone oxime Zeotiles and Zeogrids exhibit activity and selectivity similar to silicalite-1. In most of the investigated molecular separations and catalyzed reactions, Zeogrids and Zeotiles behave differently from reference zeolites and ordered mesoporous materials. The dual porosity of Zeogrids and Zeotiles presents particular advantages.

Acknowledgments

This work has been supported by the Flemish Government in Strategic Basic Research (SBO) and long-term structural funding (Methusalem) and by FWO (WOG, project funding and fellowships). CEAK acknowledges support from Prodex Belgium and ESA. Support from the Belgian Government in interuniversity attraction poles (IAP-PAI) is highly appreciated. G. Gagea, H. Vandepitte and C. Bouvier contributed specific experimental data.

References

[1] C.J. Brinker, Curr. Opin. Solid State Mater. Sci. 1 (1996) 798.
[2] J.A. Martens, P.A. Jacobs, Adv. Funct. Mater. 11 (2001) 337.
[3] R. Srivastava, M. Choi, R. Ryoo, Chem. Commun. (2006) 4489.
[4] J. Pérez-Ramírez, C.H. Christensen, K. Egeblad, C.H. Christensen, J.C. Groen, Chem. Soc. Rev. 37 (2008) 2530.
[5] R. Chal, C. Gerardin, M. Bulut, S. van Donk, ChemCatChem (2010), doi:10.1002/cctc.201000158.
[6] L. Tosheva, V.P. Valtchev, Chem. Mater. 17 (2005) 2494.
[7] A.H. Janssen, A.J. Koster, K.P. de Jong, Angew. Chem. Int. Ed. 40 (2001) 1102.
[8] J.C. Groen, L.A.A. Peffer, J.A. Moulijn, J. Pérez-Ramírez, Chem. Eur. J. 11 (2005) 4983.
[9] C.J.H. Jacobsen, C. Madsen, J. Houzvicka, I. Schmidt, A. Carlsson, J. Am. Chem. Soc. 122 (2000) 7116.
[10] Y. Liu, W. Zhang, T.J. Pinnavaia, J. Am. Chem. Soc. 122 (2000) 8791.
[11] A.E. Persson, B.J. Schoeman, J. Sterte, J.E. Otterstedt, Zeolites 14 (1994) 557.
[12] R. Ravishankar, C. Kirschhock, B.J. Schoeman, P. Vanoppen, P.J. Grobet, S. Storck, W.F. Maier, J.A. Martens, F.C. De Schryver, P.A. Jacobs, J. Phys. Chem. B 102 (1998) 2633.
[13] R. Ravishankar, C.E.A. Kirschhock, P.P. Knops-Gerrits, E.J.P. Feijen, P.J. Grobet, P. Vanoppen, F.C. De Schryver, G. Miehe, H. Fuess, B.J. Schoeman, P.A. Jacobs, J.A. Martens, J. Phys. Chem. B 103 (1999) 4960.
[14] C.E.A. Kirschhock, S.P.B. Kremer, J. Vermant, G. Van Tendeloo, P.A. Jacobs, J.A. Martens, Chem. Eur. J. 11 (2005) 4306.
[15] S. Kremer, C. Kirschhock, M. Tielen, F. Collignon, P. Grobet, P. Jacobs, J. Martens, Adv. Funct. Mater. 12 (2002) 286.
[16] S.P.B. Kremer, C.E.A. Kirschhock, A. Aerts, K. Villani, J.A. Martens, O.I. Lebedev, G.V. Tendeloo, Adv. Mater. 15 (2003) 1705.
[17] http://www.iza-structure.org/databases/.
[18] G.T. Kokotailo, S.L. Lawton, D.H. Olson, W.M. Meirer, Nature 272 (1978) 437.
[19] E.M. Flanigen, J.M. Bennett, R.W. Grose, J.P. Cohen, R.L. Patton, R.M. Kirchner, J.V. Smith, Nature 271 (1978) 512.
[20] P.A. Jacobs, J.A. Martens, Studies in Surface Science and Catalysis, vol. 33, Elsevier, Amsterdam/Oxford/New York/Tokyo, 1987, 390 pp.
[21] C.S. Cundy, P.A. Cox, Chem. Rev. 103 (2003) 663.
[22] A. Aerts, C.E.A. Kirschhock, J.A. Martens, Chem. Soc. Rev. 39 (12) (2010) 4626.
[23] T. Verstraelen, V. Van Speybroeck, M. Waroquier, J. Chem. Inf. Model. 48 (2008) 1530.
[24] http://molmod.ugent.be/code/wiki.
[25] B. Szyja, A. Jansen, T. Verstraelen, R. van Santen, Phys. Chem. Chem. Phys. 11 (35) (2009) 7605.
[26] B.J. Schoeman, O. Regev, Zeolites 17 (1996) 447.
[27] J.D. Rimer, D. Vlachos, R.F. Lobo, J. Phys. Chem. B 109 (2005) 12762.
[28] C.E.A. Kirschhock, R. Ravishankar, F. Verspeurt, P.J. Grobet, P.A. Jacobs, J.A. Martens, J. Phys. Chem. B 103 (1999) 4965.
[29] S.L. Burkett, M.E. Davis, Chem. Mater. 7 (1995) 920.
[30] W.H. Dokter, H.F. van Garderen, T.P.M. Beelen, R.A. van Santen, W. Bras, Angew. Chem. 107 (1995) 122.
[31] M. Haouas, D.P. Petry, M.W. Anderson, F. Taulelle, J. Phys. Chem. C 113 (2009) 10838.
[32] D. Lesthaeghe, P. Vansteenkiste, T. Verstraelen, C.E.A. An Ghysels, J.A. Kirschhock, V. Martens, M. Van Speybroeck, Waroquier, J. Phys. Chem. C 112 (2008) 9186.
[33] C.E.A. Kirschhock, R. Ravishankar, P.A. Jacobs, J.A. Martens, J. Phys. Chem. B 103 (1999) 11021.
[34] A. Aerts, L.R.A. Follens, M. Haouas, T.P. Caremans, M.A. Delsuc, B. Loppinet, J. Vermant, B. Goderis, F. Taulelle, J.A. Martens, C.E.A. Kirschhock, Chem. Mater. 19 (2007) 3448.
[35] D. Liang, L.R.A. Follens, A. Aerts, J.A. Martens, G. Van Tendeloo, C.E.A. Kirschhock, J. Phys. Chem. C 111 (2007) 14283.
[36] T.M. Davis, T.O. Drews, H. Ramanan, C. He, J. Dong, H. Schnablegger, M.A. Katsoulakis, E. Kokkoli, A.V. Mccormick, R.L. Penn, M. Tsapatsis, Nat. Mater. 5 (2006) 400.
[37] C.E.A. Kirschhock, V. Buschmann, S. Kremer, R. Ravishankar, C.J.Y. Houssin, B.L. Mojet, R.A. van Santen, P.J. Grobet, P.A. Jacobs, J.A. Martens, Angew. Chem. Int. Ed. 40 (2001) 2637.
[38] A. Aerts, W. Huybrechts, S.P.B. Kremer, C.E.A. Kirschhock, E. Theunissen, A. Van Isacker, J.F.M. Denayer, G.V. Baron, J.W. Thybaut, G.B. Marin, P.A. Jacobs, J.A. Martens, Chem. Commun. (2003) 1888.
[39] T. Verstraelen, B.M. Szyja, D. Lesthaeghe, R. Declerck, V. Van Speybroeck, M. Waroquier, A.P.J. Jansen, A. Aerts, L.R.A. Follens, J.A. Martens, C.E.A. Kirschhock, R.A. van Santen, Top. Catal. 52 (2009) 1261.
[40] P.C.M.M. Magusin, V.E. Zorin, A. Aerts, C.J.Y. Houssin, A.L. Yakovlev, C.E.A. Kirschhock, J.A. Martens, R.A. van Santen, J. Phys. Chem. B 109 (2005) 22767.
[41] C.E.A. Kirschhock, R. Ravishankar, L. Van Looveren, P.A. Jacobs, J.A. Martens, J. Phys. Chem. B 103 (1999) 4972.
[42] S.P.B. Kremer, C.E.A. Kirschhock, P.A. Jacobs, J.A. Martens, C. R. Chim. 8 (2005) 379.
[43] S.P.B. Kremer, C.E.A. Kirschhock, M. Tielen, F. Collignon, P.J. Grobet, P.A. Jacobs, J.A. Martens, Stud. Surf. Sci. Catal. 143 (2002) 185.
[44] A. Aerts, A. van Isacker, W. Huybrechts, S.P.B. Kremer, C.E.A. Kirschhock, F. Collignon, K. Houthoofd, J.F.M. Denayer, G.V. Baron, G.B. Marin, P.A. Jacobs, J.A. Martens, Appl. Catal. A 257 (2004) 7.
[45] A. Aerts, W. Huybrechts, S.P.B. Kremer, C.E.A. Kirschhock, E. Theunissen, A. Van Isacker, J.F.M. Denayer, G.V. Baron, J.W. Thybaut, G.B. Marin, P.A. Jacobs, J.A. Martens, Chem. Commun. (2003) 1888.
[46] S.P.B. Kremer, C.E.A. Kirschhock, A. Aerts, C.A. Aerts, K.J. Houthoofd, P.J. Grobet, P.A. Jacobs, O.I. Lebedev, G. Van Tendeloo, J.A. Martens, Solid State Sci. 7 (2005) 861.
[47] S. Bals, K.J. Batenburg, D. Liang, O. Lebedev, G.V. Tendeloo, A. Aerts, J.A. Martens, C.E.A. Kirschhock, J. Am. Chem. Soc. 131 (2009) 4769.
[48] E. Theunissen, C.E.A. Kirschhock, S.P.B. Kremer, D.D. Habermacher, J.A. Martens, Eur. J. Inorg. Chem. (2003) 1296.
[49] M. Reichinger, W. Schmidt, M.W.E. van den Berg, A. Aerts, J.A. Martens, C.E.A. Kirschhock, H. Gies, W. Grünert, J. Catal. 269 (2010) 367.
[50] L.I. Devriese, L. Cools, A. Aerts, J.A. Martens, G.V. Baron, J.F.M. Denayer, Adv. Funct. Mater. 17 (2007) 3911.
[51] F. Xu, Y.J. Wang, X.D. Wang, Y.H. Zhang, Y. Tang, P.Y. Yang, Adv. Mater. 15 (2003) 1751.
[52] T. Yasmin, K. Muller, J. Chromatogr. A 1217 (2010) 3362.
[53] A. Galarneau, J. Lapichella, D. Brunel, F. Fajula, Z. Bayram-Hahn, K. Unger, G. Puy, C. Demesmay, J.L. Rocca, J. Sep. Sci. 29 (2006) 844.
[54] A. Kurganov, K. Unger, T. Issaeva, J. Chromatogr. A 753 (1996) 177.
[55] M. Raimondo, G. Perez, N. Sinibaldi, A. DeStefanis, A.A.G. Tomlinson, Chem. Commun. (1997) 1343.
[56] C. Thoelen, K. Van de Walle, I.F.J. Vankelecom, P.A. Jacobs, Chem. Commun. (1999) 1841.
[57] T. Martin, A. Galarneau, F. Di Renzo, D. Brunel, F. Fajula, S. Heinisch, G. Cretier, J.L. Rocca, Chem. Mater. 16 (2004) 1725.
[58] A. Galarneau, J. Iapichella, K. Bonhomme, F. Di Renzo, P. Kooyman, O. Terasaki, F. Fajula, Adv. Funct. Mater. 16 (2006) 1657.
[59] B. Dejaegher, S. Pieters, Y. Heyden, Comb. Chem. High Throughput Screen. 13 (2010) 530.
[60] M. Tagliabue, D. Farrusseng, S. Valencia, S. Aguado, U. Ravon, C. Rizzo, A. Corma, C. Mirodatos, Chem. Eng. J. 155 (2009) 553.
[61] J. Caro, M. Noack, P. Kölsch, R. Schäfer, Micropor. Mesopor. Mater. 38 (2000) 3.
[62] T. Van Gestel, C. Vandecasteele, A. Buekenhoudt, C. Dotremont, J. Luyten, R. Leysen, B. Van der Bruggen, G. Maes, J. Membr. Sci. 207 (2002) 73.
[63] J.A. Martens, M. Tielen, P.A. Jacobs, J. Weitkamp, Zeolites 4 (1984) 98.
[64] J. Weitkamp, P.A. Jacobs, J.A. Martens, Appl. Catal. 8 (1983) 123.
[65] D. Dubbeldam, S. Calero, T.L.M. Maesen, B. Smit, Angew. Chem. Int. Ed. 42 (2003) 3624.

[66] J.A. Martens, R. Parton, L. Uytterhoeven, P.A. Jacobs, G.F. Froment, Appl. Catal. 76 (1991) 95.
[67] C. Bouvier, W. Buijs, J. Gascon, F. Kapteijn, B.C. Gagea, P.A. Jacobs, J.A. Martens, J. Catal. 270 (2010) 60.
[68] R. Van Borm, A. Aerts, M. Reyniers, J.A. Martens, G.B. Marin, Ind. Eng. Chem. Res. 49 (2010) 6815.
[69] R. Van Borm, M. Reyniers, J.A. Martens, G.B. Marin, Ind. Eng. Chem. Res. 49 (2010) 10486.
[70] R. Quintana-Solorzano, J.W. Thybaut, G.B. Marin, Appl. Catal. A: Gen. 314 (2006) 184.
[71] R. Quintana-Solórzano, J.W. Thybaut, G.B. Marin, Chem. Eng. Sci. 62 (2006) 5033.
[72] C.B. Khouw, C.B. Dartt, J.A. Labinger, M.E. Davis, J. Catal. 149 (1994) 195.
[73] P. Ratnasamy, D. Srinivas, H. Knozinger, Adv. Catal. 48 (2004) 1.
[74] G. Dahlhoff, J.P.M. Niederer, W.F. Hoelderich, Catal. Rev.—Sci. Eng. 43 (2001) 381.